Regularly arranged indium islands on glass/molybdenum substrates upon femtosecond laser and physical vapor deposition processing

F. Ringleb,[1] K. Eylers,[1] Th. Teubner,[1] T. Boeck,[1,a)] C. Symietz,[2] J. Bonse,[2] S. Andree,[2] J. Krüger,[2] B. Heidmann,[3,4] M. Schmid,[3,4] and M. Lux-Steiner[4,5]
[1]*Leibniz-Institute for Crystal Growth, Max-Born-Straße 2, Berlin 12489, Germany*
[2]*Bundesanstalt für Materialforschung und-prüfung (BAM), Unter den Eichen 87, Berlin 12205, Germany*
[3]*Department of Physics, Freie Universität Berlin, Arnimalle 14, Berlin 14195, Germany*
[4]*Nanooptical Concepts for PV, Helmholtz Zentrum Berlin, Hahn-Meitner-Platz 1, Berlin 14109, Germany*
[5]*Heterogeneous Material Systems, Helmholtz Zentrum Berlin, Hahn-Meitner-Platz 1, Berlin 14109, Germany*

(Received 6 January 2016; accepted 1 March 2016; published online 17 March 2016)

A bottom-up approach is presented for the production of arrays of indium islands on a molybdenum layer on glass, which can serve as micro-sized precursors for indium compounds such as copper-indium-gallium-diselenide used in photovoltaics. Femtosecond laser ablation of glass and a subsequent deposition of a molybdenum film or direct laser processing of the molybdenum film both allow the preferential nucleation and growth of indium islands at the predefined locations in a following indium-based physical vapor deposition (PVD) process. A proper choice of laser and deposition parameters ensures the controlled growth of indium islands exclusively at the laser ablated spots. Based on a statistical analysis, these results are compared to the non-structured molybdenum surface, leading to randomly grown indium islands after PVD. © *2016 AIP Publishing LLC*.
[http://dx.doi.org/10.1063/1.4943794]

Indium compounds such as indium phosphide (InP), indium arsenide (InAs), and indium tin oxide (ITO) play an important role for a broad range of electronic and optoelectronic applications. Moreover, indium is a constituent of copper-indium-gallium-diselenide (CIGSe), which is an excellent direct optical absorber in the visible spectral range, and is therefore applied in highly efficient thin film solar cells.[1] However, due to the rareness of indium, large efforts are being made to develop material-saving manufacturing processes and technologies, as well as efficient recycling procedures.[2–4]

Sophisticated solar cell architectures including a concentrator design can achieve material saving along with increased solar cell conversion efficiencies. Since the active absorber area is reduced under concentrated illumination, the required amount of material decreases. Compared to macroscopic concentrator solar cells, their microscopic counterparts exhibit a better heat dissipation due to a higher surface to volume ratio and, therefore, reduced thermal losses. An approach for the preparation of microconcentrator cells has been demonstrated for silicon.[5]

The microconcentrator concept is particularly interesting for thin film systems, which were previously limited to the low concentration regime (illumination at 1–10 suns) due to excessive resistive losses and a difficult thermal management.[6] Encouraging proof-of-principle CIGSe model microconcentrator solar cells have been reported. In the corresponding top-down studies, microabsorbers were prepared from CIGSe films by lithography and tested for a broad range of concentration factors.[6–9] Paire *et al.* achieved an absolute efficiency enhancement of up to 5% at 475 suns and an equivalent efficiency of 21.3% for a 50 μm diameter cell.[8] However, a material saving bottom-up process for the preparation of CIGSe microstructures has to be developed.

The preparation of regularly ordered microstructures on substrates can be realized by pulsed laser processing.[10] This technology takes benefit of the contactless treatment and is straightforward to be implemented in industrial photovoltaic manufacturing. On the standard back contact material for CIGSe cells, molybdenum, indium exhibits a strong tendency for three-dimensional island growth.[11] In this work, we present a procedure for the *spatially controlled* nucleation and formation of indium islands by applying femtosecond (fs) laser pulses with energy densities (fluences) near the ablation threshold of the substrate for realizing only subtle changes in the sample morphology.

Commercial $50 \times 50 \times 2\,\mathrm{mm}^3$ soda-lime floatglass samples (*Weidner Glas*, part number 449004) served as substrates. Sequential metal deposition was carried out by physical vapor deposition (PVD) in a high vacuum chamber (*Edwards*, Auto 306, FL 400) with a base pressure of 10^{-6} mbar. The samples facing down with their front side towards the evaporator were fixed with the backside to a custom-built all-ceramic heating plate (*BACH Resistor Ceramics*). In addition, the samples were heated from the front by a set of four halogen lamps (*Osram*, Xenophot HLX 64653). Their temperature was measured by thermocouples pressed to the backside of the heating plate. Both molybdenum and indium were deposited at a substrate temperature of 510 °C. Deposition rates and film thicknesses were measured by a quartz microbalance and a rate/thickness monitor (*Inficon* SQM-160). Molybdenum films of 320–420 nm thickness were deposited at rates between 1 and 1.8 Å/s. The layer thickness of indium, which was in the range of 80–100 nm, has merely a nominal meaning due to the formation of islands during deposition.

a)Author to whom correspondence should be addressed. Electronic mail: torsten.boeck@ikz-berlin.de

In order to fabricate well-defined indium arrays, laser-based substrate patterning was carried out at ambient atmosphere by a pulsed Ti:Sapphire fs-laser (*Femtolasers*, Compact Pro) with a center wavelength of 790 nm, a pulse duration of 30 fs, and a maximum repetition rate of 1 kHz. The laser beam was directly focused to the substrate by a spherical mirror, resulting in a Gaussian beam profile with a radius $w_0 \sim 100$–$130\ \mu$m at the surface. The number of pulses per surface spot varied from 1 to 1000. The patterning was restricted to an area of $16 \times 16\,\text{mm}^2$ such that a large part of the substrate remained unmodified.

Two different approaches of laser-based substrate patterning were realized. In the first configuration [Figure 1, process I], the glass substrate was laser-structured (step 1) before the molybdenum layer (step 2) and indium (step 3) were both deposited by PVD. The second configuration [Figure 1, process II] comprised the deposition of molybdenum on the pristine glass substrate by PVD (step 1), a subsequent laser treatment of the molybdenum layer (step 2), and finally the PVD of indium (step 3).

Optical microscopy was carried out in brightfield mode with a *Reichert Polyvar 2* microscope equipped with a CCD camera (*Nikon* DS-5M), a DS-U1 interface and NIS-Elements F imaging software (version 3.22). Statistical analysis of the areal distribution of indium islands was realized using the image analysis software imageJ (version 1.49) with a self-written script for automated image processing. Nearest neighbor distributions (NNDs) were determined by the calculation of the Euclidean distances of the center points of the islands, i.e., the average values of the *x*- and *y*-coordinates of all pixels belonging to an individual island. Scanning electron microscopic (SEM) investigations were carried out with a *Nova 600 Nanolab DualBeam* microscope from *FEI*. Atomic-force microscopic (AFM) data were obtained using a *Dimension Icon* microscope (*Bruker*), operated in the tapping mode.

The application of fs-laser pulses leads to sharply localized surface modifications of the target. A strong impact leads to unwanted deep ablation structures. This work focuses on using peak fluences just above ablation threshold resulting in very subtle changes in the substrate morphology. The aim is to produce only as much as necessary change of the surface to initiate nucleation sites for the growth of indium islands.

Figure 2 demonstrates, as proof-of-principle, the site-selective ablation of glass [Figure 2(a)], followed by the PVD of a 420 nm thick molybdenum layer and indium islands within the laser crater [Figure 2(b)]. The laser spot was prepared by process I, using 100 pulses at a peak fluence of $1.6\,\text{J/cm}^2$ [Figure 2(a)]. The spatial Gaussian profile of the focused laser beam caused the formation of surface ablation spots with the strongest changes in the center. A clear threshold behavior of ablation can be observed. The curve provided in the lower part of Figure 2(a) shows an AFM cross-sectional profile of the laser spot surface topography. It exhibits a maximum depth of ~300 nm in the center. In general, the profiles can be described as the superposition of a shallow parabola (depth: 0.25 μm and width: 50 μm) and an additional contribution with a roughness parameter R_a of ca. 25 nm, averaged over the entire profile. The preferential nucleation of indium in such laser-patterned spots is evidenced in Figure 2(b). This figure shows an SEM micrograph of a laser spot after deposition of the molybdenum and indium. The inset in Figure 2(b) clearly shows characteristic laser-induced periodic surface structures, which are commonly formed at fluences close to

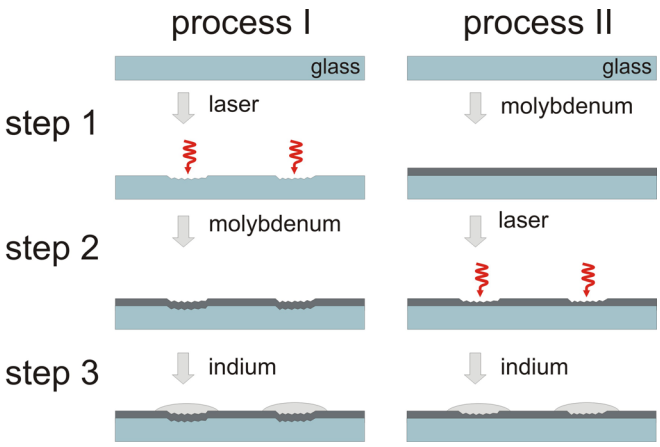

FIG. 1. Scheme of two different routes of substrate preparation. Process I: Laser patterning of glass substrate (step 1) followed by molybdenum layer (step 2) and indium island deposition (step 3). Process II: Deposition of molybdenum layer onto glass substrate (step 1) followed by laser patterning (step 2) and indium island deposition (step 3).

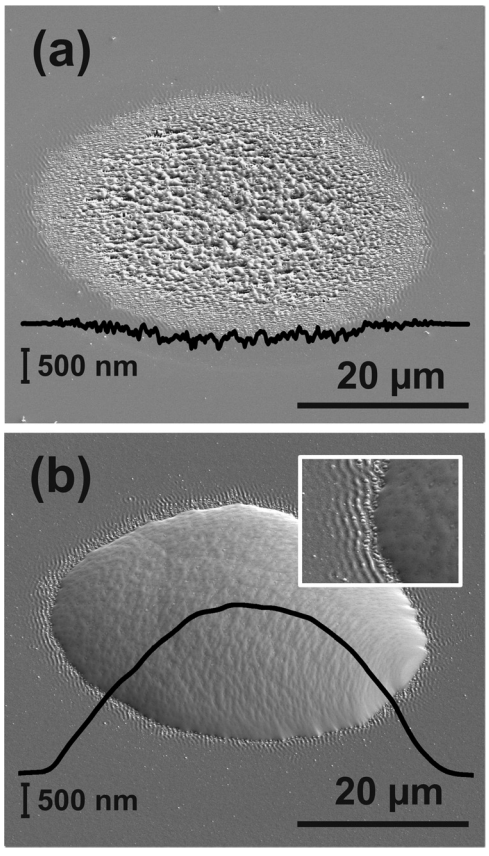

FIG. 2. SEM micrographs of a single fs-laser ablation spot on glass prior to (a) and after deposition of molybdenum and indium (b). SEM-view tilted by 52° with respect to surface normal. (a) Process I, after step 1. To ensure conductivity, 40 nm of molybdenum were deposited onto this sample prior to SEM imaging. The curve in (a) represents an AFM cross section through the crater profile. (b) Process I, after step 3. The curve in (b) represents a profilometric scan across the center of the indium island. The inset in (b) shows a detailed magnification of the indium-molybdenum transition zone.

the ablation threshold.[12] The indium island diameter, geometrical aspect ratio, and nucleation density all depend on the deposition rate and temperature. The indium deposition conditions applied here (nominal deposition rate: 0.3 Å/s; nominal film thickness: 100 nm) were optimized in order to meet the geometrical requirements of microconcentrator cells. A surface profilometric measurement of such an indium island is shown in the lower part of Figure 2(b) and reveals a height of 2.6 μm along with a diameter of 45 μm and therefore a height-to-width aspect ratio of 0.06.

The large area optical micrograph [Figure 3(a)] shows a whole array of laser processed spots with subsequent indium deposition. Each dark spot corresponds to an indium island as previously shown in Figure 2(b). Within the array area, indium island growth takes place exclusively at the predefined spots, i.e., no islands are found elsewhere. In contrast, Figure 3(b) shows a non-patterned region of the same molybdenum-covered glass sample where the islands are distributed statistically.

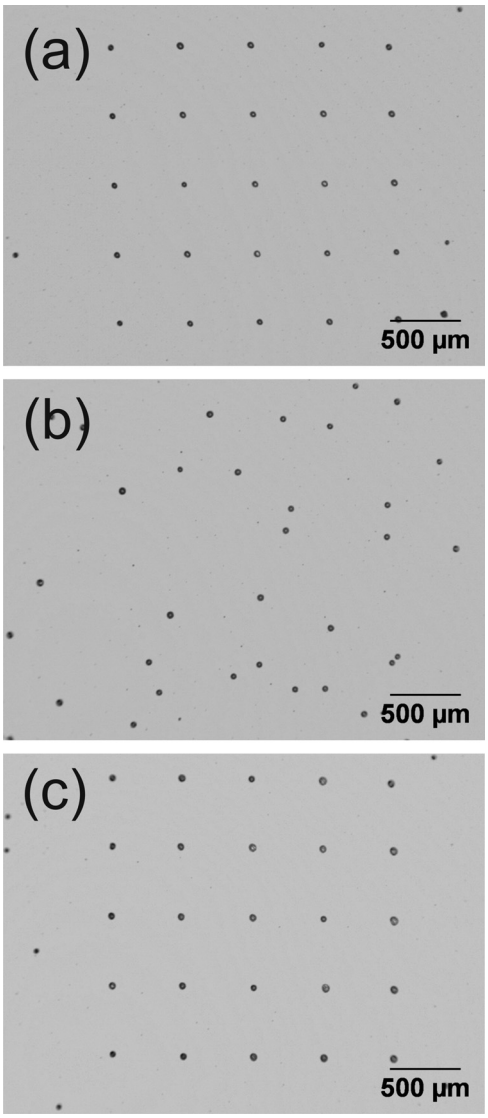

FIG. 3. Optical micrographs showing the formation of indium islands on molybdenum coated glass substrates. (a) Laser-based process I: 5 × 5 array with 500 μm spacing. (b) Reference area outside of the laser-patterned region showing a random distribution of indium islands. (c) Laser-based process II: 5 × 5 array with 500 μm spacing.

In order to study the impact of the order of laser processing and molybdenum deposition, the alternative process II was studied, i.e., the molybdenum-covered glass was laser structured prior to the indium PVD. Figure 3(c) shows indium islands deposited by process II. Here, the glass substrate was first covered with 320 nm of molybdenum. Subsequently, the surface was patterned again with 5 × 5 arrays of laser spots (pulse number = 10, peak fluence = 0.2 J/cm^2) before indium was deposited at a rate of 0.25 Å/s resulting in a nominal thickness of 90 nm. Note that different laser parameters were used for both processes (compare Figure 1) due to the different interaction between the laser radiation and glass or molybdenum. The comparison of Figures 3(a) and 3(c) evidences that both approaches are suitable to induce the locally controlled growth of indium islands at the laser spots.

It is known that in addition to tailoring the topography, fs-laser irradiation may lead to structural and chemical changes at the surface, such as amorphization,[13] alterations of chemical bond-lengths,[14] oxidation,[15] etc. However, these changes become irrelevant, when a molybdenum film of several hundred nanometer thickness is deposited onto the laser-processed surface (process I). Both processes (I and II) comprise a laser-induced roughening, while only process II may be influenced by additional chemical effects. Obviously, solely a morphological modification of the substrate is sufficient to act as a material trap.

In order to determine to what extent the ablation crater geometry affects the indium island growth process, the laser processing parameters were systematically varied. This aims to obtain smooth and symmetric indium islands potentially suitable as a first building block for realizing CIGSe microconcentrator solar cells. The SEM images shown in Figure 4 summarize the influence of pulse number (between 1 and 1000) and peak fluence (between 1.4 and 3.0 J/cm^2) on the resulting indium microstructures. In this experiment (process I), the glass substrate was patterned before 420 nm of molybdenum and 100 nm of indium (rate = 0.35 Å/s) were deposited. Figure 4(c) clearly illustrates, that in the regime of strong material ablation at high pulse numbers and high fluences, a deep crater is formed. Even though indium accumulates here,

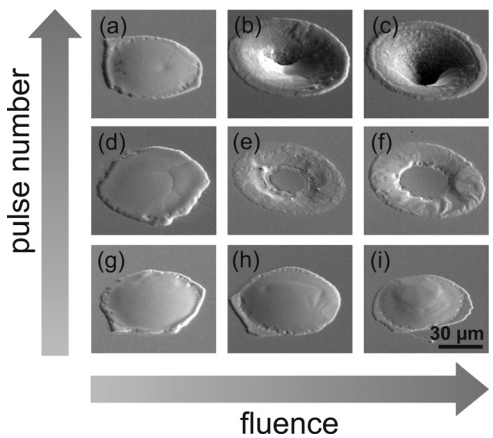

FIG. 4. Collage of SEM micrographs demonstrating the influence of laser parameters (process I). Pulse numbers: (a): 300; (b) and (c): 1000; (d)–(f): 30; (g)–(i): 1. Peak fluences (J/cm^2): (a): 1.4, (b): 1.7, (c): 1.9, (d): 1.8, (e): 2.0, (f): 2.5, (g): 2.3, (h): 2.6, and (i): 3.0. SEM-view tilted 52° with respect to surface normal.

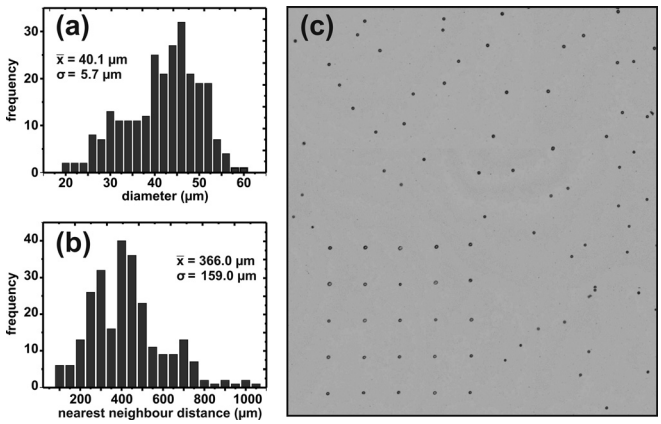

FIG. 5. Indium island distribution outside of the patterned zone. (a) Statistical analysis of island diameter. (b) Statistical analysis of the nearest neighbor distance. (c) Optical micrograph of the transition zone between the laser-patterned and non-patterned regions (array spacing: 500 μm). Number of analyzed islands: 227.

this treatment does not lead to the desired flat, mesa-shaped islands. Intermediate material ablation such as visible in Figures 4(e) and 4(f) result in flat rings, but still, the morphological distortion is too strong to allow the formation of a homogeneous island. Indeed, the best results are obtained for the softest laser parameters, which lead to minor material removal along with a surface roughening. Even the mildest treatment [Figure 4(g): 1 pulse, 2.3 J/cm^2] was sufficient to result in preferential and exclusive nucleation at the corresponding spot. The islands, which resemble most the desired mesa shape [Figures 4(a), 4(d), 4(g), and 4(h)], all exhibit the same morphology as the islands grown outside of the laser-spot array. This indicates that the corresponding laser treatment influences the nucleation of islands but has no effect on the resulting island shape.

In all experiments reported here, the $50 \times 50\,\text{mm}^2$ substrates were patterned at maximum in an area of $16 \times 16\,\text{mm}^2$. Hence, a large fraction of the substrate remained unmodified. The indium island distribution of the "unperturbed" surface area was statistically analyzed. Figure 5 shows a sample, where 90 nm of indium were deposited at a rate of 0.25 Å/s onto a laser-patterned molybdenum film of 320 nm thickness (process II of Figure 1). The resulting indium islands—the statistical sample size was 227 islands—exhibit an average diameter of 40 μm and an average nearest neighbor distance (NND) of 366 μm. The relative standard deviation of the NND (0.43) is much higher than that of the island diameter (0.14), i.e., even though the islands are distributed irregularly, they are of similar size. Figure 5(c) gives an overview of a laser-patterned region (pulse number = 10, peak fluence = 0.2 J/cm^2), the adjacent transition zone and the surrounding non-patterned area. It is interesting to note, that even though the NND in the non-patterned area is smaller (366 μm) than the spacing of the laser spots within the arrays (500 μm), the islands are ordered efficiently in the patterned region and undesired nucleation in between the laser spots is not observed. Moreover, the areal density of the islands within the transition zone, which comprises several hundred micrometers, is reduced compared to that of the non-patterned region further away from the array. Apparently, the lower nucleation energy required on the laser spots leads to the formation of islands. Their capture zones for material diffusing on the surface leads to an initial depletion of indium and therefore suppresses further nucleation in the nearer surrounding of the array. The NND of droplets within the non-patterned area provides a good measure for a suitable array spacing. Exclusive island growth at the laser spots is still very efficient even when the spot spacing is in the range of—or slightly higher than—the mean NND. Note that the high NND standard deviation means that a large fraction of islands has also a closer nearest neighbor.

In summary, substrate patterning by fs-laser pulses is a suitable technique for creating preferred nucleation sites for the growth of regularly arranged indium island on a molybdenum layer. Both processes investigated here, i.e., patterning of the molybdenum layer or patterning of the underlying glass substrate, yielded the desired result of well-defined arrays of indium islands without island growth in between the laser spots. Therefore, a purely morphological surface modification is sufficient for the creation of preferential nucleation centers, whereas potential chemical surface modifications (laser-induced oxidation) do not affect the geometrically stimulated nucleation process. A very subtle substrate modification is sufficient to induce preferential island growth at the predefined spots. The distance between the laser spots can be as large as, or even slightly higher than, the average nearest neighbor distance of islands on a non-patterned substrate.

The authors gratefully acknowledge financial support from the Deutsche Forschungsgemeinschaft (DFG) through BO 1129/6-1, KR 3638/3-1, and SCHM 2554/3-1. The research leading to these results has received funding from the European Union Seventh Framework Programme (FP7/2007-2013) under Grant Agreement No. 609788.

[1]P. Jackson, D. Hariskos, R. Wuerz, O. Kiowski, A. Bauer, T. M. Friedlmeier, and M. Powalla, Phys. Status Solidi RRL **9**, 28 (2015).
[2]C. H. Lee, M. K. Jeong, M. F. Kilicaslan, J. H. Lee, H. S. Hong, and S. J. Hong, Waste Manage. **33**, 730 (2013).
[3]H. N. Kang, J. Y. Lee, and J. Y. Kim, Hydrometallurgy **110**, 120 (2011).
[4]Y. Li, Z. Liu, Q. Li, Z. Liu, and L. Zeng, Hydrometallurgy **105**, 207 (2011).
[5]J. Yoon, A. J. Baca, S. I. Park, P. Elvkis, J. B. Geddes, L. F. Li, R. H. Kim, J. L. Xiao, S. D. Wang, T. H. Kim, M. J. Motala, B. Y. Ahn, E. B. Duoss, J. A. Lewis, R. G. Nuzzo, P. M. Ferreira, Y. G. Huang, A. Rockett, and J. A. Rogers, Nat. Mater. **7**, 907 (2008).
[6]M. Paire, A. Shams, L. Lombez, N. Pere-Laperne, S. Collin, J. L. Pelauard, J. F. Guillemoles, and D. Lincot, Energy Environ. Sci. **4**, 4972 (2011).
[7]B. Reinhold, M. Schmid, D. Greiner, M. Schüle, D. Kieven, A. Ennaoui, and M. C. Lux-Steiner, Prog. Photovoltaics Res. Appl. **23**, 1929 (2015).
[8]M. Paire, L. Lombez, F. Donsanti, M. Jubault, S. Collin, J. L. Pelauard, J. F. Guillemoles, and D. Lincot, J. Renewable Sustainable Energy **5**, 011202 (2013).
[9]M. Paire, C. Jeanm, L. Lombez, S. Collin, J. L. Pelauard, I. Gerard, J. F. Guillemoles, and D. Lincot, Thin Solid Films **582**, 258 (2015).
[10]D. Bäuerle, *Laser Processing and Chemistry*, 4th ed. (Springer, Heidelberg, 2011).
[11]M. Block, R. Kunert, E. Schöll, T. Boeck, and Th. Teubner, New J. Phys. **6**, 166 (2004).
[12]J. Bonse, J. Krüger, S. Höhm, and A. Rosenfeld, J. Laser Appl. **24**, 042006 (2012).
[13]J. Bonse, S. M. Wiggins, and J. Solis, J. Appl. Phys. **96**, 2352 (2004).
[14]T. Seuthe, M. Höfner, F. Reinhardt, W. J. Tsai, J. Bonse, M. Eberstein, H. J. Eichler, and M. Grehn, Appl. Phys. Lett. **100**, 224101 (2012).
[15]J. Bonse and J. Krüger, J. Appl. Phys. **107**, 054902 (2010).